

Band offsets in complex-oxide thin films and heterostructures of SrTiO₃/LaNiO₃ and SrTiO₃/GdTiO₃ by soft and hard X-ray photoelectron spectroscopy

G. Conti, A. M. Kaiser, A. X. Gray, S. Nemšák, G. K. Pálsson, J. Son, P. Moetakef, A. Janotti, L. Bjaalie, C. S. Conlon, D. Eiteneer, A. A. Greer, A. Keqi, A. Rattanachata, A. Y. Saw, A. Bostwick, W. C. Stolte, A. Gloskovskii, W. Drube, S. Ueda, M. Kobata, K. Kobayashi, C. G. Van de Walle, S. Stemmer, C. M. Schneider, and C. S. Fadley

Citation: *Journal of Applied Physics* **113**, 143704 (2013); doi: 10.1063/1.4795612

View online: <http://dx.doi.org/10.1063/1.4795612>

View Table of Contents: <http://scitation.aip.org/content/aip/journal/jap/113/14?ver=pdfcov>

Published by the AIP Publishing

Articles you may be interested in

[Near-nanoscale-resolved energy band structure of LaNiO₃/La₂/3Sr₁/3MnO₃/SrTiO₃ heterostructures and their interfaces](#)

J. Vac. Sci. Technol. B **33**, 04E103 (2015); 10.1116/1.4922270

[Insulating-layer formation of metallic LaNiO₃ on Nb-doped SrTiO₃ substrate](#)

Appl. Phys. Lett. **106**, 121601 (2015); 10.1063/1.4916225

[Observation of strontium segregation in LaAlO₃/SrTiO₃ and NdGaO₃/SrTiO₃ oxide heterostructures by X-ray photoemission spectroscopy](#)

APL Mat. **2**, 012108 (2014); 10.1063/1.4861797

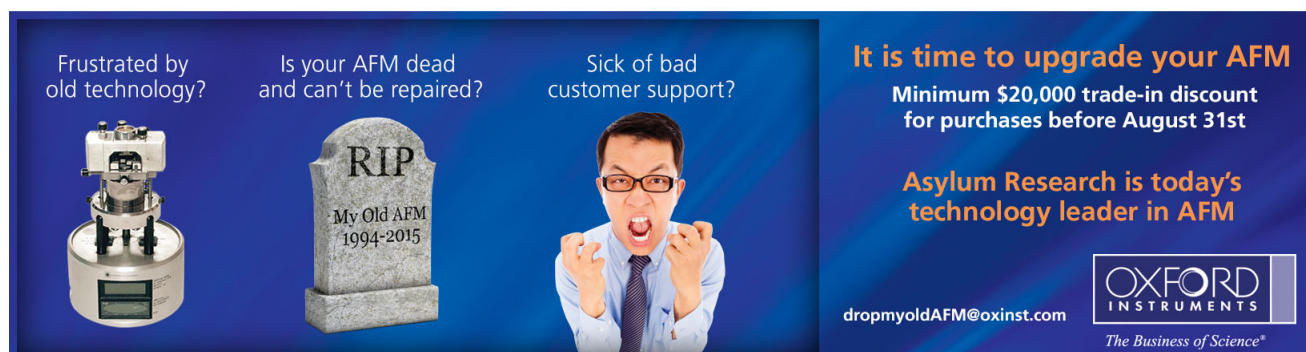
[Capacitance-voltage analysis of high-carrier-density SrTiO₃/GdTiO₃ heterostructures](#)

Appl. Phys. Lett. **100**, 232106 (2012); 10.1063/1.4726263


[Correlation of high temperature x-ray photoemission valence band spectra and conductivity in strained LaSrFeNi oxide on SrTiO₃ \(110\)](#)

Appl. Phys. Lett. **95**, 022107 (2009); 10.1063/1.3174916


Frustrated by old technology?



Is your AFM dead and can't be repaired?



Sick of bad customer support?




It is time to upgrade your AFM

Minimum \$20,000 trade-in discount for purchases before August 31st

Asylum Research is today's technology leader in AFM

dropmyoldAFM@oxinst.com



The Business of Science®

Band offsets in complex-oxide thin films and heterostructures of SrTiO₃/LaNiO₃ and SrTiO₃/GdTiO₃ by soft and hard X-ray photoelectron spectroscopy

G. Conti,^{1,2} A. M. Kaiser,^{1,2,3,a)} A. X. Gray,^{1,2,4} S. Nemšák,^{1,2} G. K. Pálsson,^{1,2} J. Son,⁵ P. Moetakef,⁵ A. Janotti,⁵ L. Bjaalie,⁵ C. S. Conlon,^{1,2} D. Eiteneer,^{1,2} A. A. Greer,^{1,6} A. Keqi,^{1,2} A. Rattanachata,^{1,2} A. Y. Saw,^{1,2} A. Bostwick,⁷ W. C. Stolte,⁷ A. Gloskovskii,⁸ W. Drube,⁸ S. Ueda,⁹ M. Kobata,¹⁰ K. Kobayashi,⁹ C. G. Van de Walle,⁵ S. Stemmer,⁵ C. M. Schneider,³ and C. S. Fadley^{1,2}

¹Department of Physics, University of California, Davis, California 95616, USA

²Materials Sciences Division, Lawrence Berkeley National Laboratory, Berkeley, California 94720, USA

³Peter-Grünberg-Institut PGI-6, Forschungszentrum Jülich, 52425 Jülich, Germany

⁴Stanford Institute for Materials and Energy Sciences, SLAC National Accelerator Laboratory, Menlo Park, California 94025, USA

⁵Materials Department, University of California, Santa Barbara, California 93106, USA

⁶Chemical Engineering and Materials Science Engineering, University of California, Davis California 95616, USA

⁷Advanced Light Source, Lawrence Berkeley National Laboratory, Berkeley, California 94720, USA

⁸Deutsches Elektronen-Synchrotron DESY, 22607 Hamburg, Germany

⁹Synchrotron X-ray Station at SPring-8, National Institute for Materials Science, Hyogo 679-5148, Japan

¹⁰Quantum Beam Science Directorate, Japan Atomic Energy Agency Kouto 1-1-1, SPring-8 Hyogo 679-5148, Japan

(Received 13 January 2013; accepted 4 March 2013; published online 8 April 2013)

The experimental determination of valence band offsets (VBOs) at interfaces in complex-oxide heterostructures using conventional soft x-ray photoelectron spectroscopy (SXPS, $h\nu \leq 1500$ eV) and reference core-level binding energies can present challenges because of surface charging when photoelectrons are emitted and insufficient probing depth to clearly resolve the interfaces. In this paper, we compare VBOs measured with SXPS and its multi-keV hard x-ray analogue (HXP, $h\nu > 2000$ eV). We demonstrate that the use of HXP allows one to minimize charging effects and to probe more deeply buried interfaces in heterostructures such as SrTiO₃/LaNiO₃ and SrTiO₃/GdTiO₃. The VBO values obtained by HXP for these interfaces are furthermore found to be close to those determined by first-principles calculations. © 2013 American Institute of Physics.

[<http://dx.doi.org/10.1063/1.4795612>]

INTRODUCTION

Multilayer (ML) structures of metals and semiconductors have been extensively studied in terms of their electronic structure, including Schottky barrier heights and band offsets.¹ Recently, new classes of heterostructures consisting of complex-oxides have attracted great interest because they possess functional properties not present in the associated bulk materials or in single layers.^{2–4} For instance, although the bulk materials composing the multilayers are insulators, their superlattices can show metallic conductivity, due to unique interfacial properties. The carrier confinement and transport properties of these heterostructures depend critically on the band lineups of buried interfaces, or equivalently on their conduction band offset (CBO) and valence band offset (VBO).⁵ How the bands offsets are distributed between the valence and conduction bands is not known *a priori* but must be experimentally or theoretically determined. The determinations of VBOs in these classes of heterostructures thus provide crucial information regarding the nature of charge transport and quantum confinement at their

interfaces, and are important for designing devices making use of these phenomena. In this article, we consider two different oxide heterostructures: SrTiO₃ (STO), a wide-gap band insulator with a bulk bandgap⁶ of 3.25 eV in contact with LaNiO₃ (LNO), a correlated metal that exhibits a metal-to-insulator transition (MIT) in sufficiently thin and strained layers;⁷ and STO in contact with GdTiO₃ (GTO), a Mott-Hubbard insulator with a small bandgap of ~ 0.8 eV.^{8,9} The latter interface exhibits a two-dimensional electron gas (2DEG) and ferromagnetism at the interface with STO.^{10,11}

X-ray photoemission spectroscopy (XPS), which provides both core- and valence-level spectra from bulk reference compounds and heterostructures, is an established technique for determining VBOs, beginning with studies of semiconductors,^{12–14} and more recently complex oxides.^{15,16} With XPS, the electrostatic potential at the interface can be monitored and the band bending and the band discontinuity of the heterostructure are determined. Compared to optical or transport methods, XPS provides a direct measurement of the band offsets, and the interpretation of the experimental results is straightforward.

In this paper, we report the VBOs of STO/LNO and STO/GTO heterostructures as determined by both traditional

^{a)}Present address: SPECS Surface Nano Analysis GmbH, Voltastraße 5, 13355 Berlin, Germany.

soft XPS (SXPS, $h\nu \leq 1500$ eV) and hard XPS (HXPS, $h\nu \geq 2000$ eV). We demonstrate the advantages of HXPS measurements in achieving a sufficient probing depth capable of fully resolving the buried interfaces in heterostructures, as well as being less susceptible to charging effects.

The experimental VBO values obtained by HXPS are compared to theoretical values estimated by first-principles calculations based on density functional theory and using a hybrid functional for the separate bulk materials and for the respective interface.^{17–19}

SAMPLES AND EXPERIMENTAL PROCEDURE

The samples, all grown in (001) orientation on $(\text{LaAlO}_3)_{0.3}(\text{Sr}_2\text{AlTaO}_6)_{0.7}$ (LSAT) substrates, were measured by SXPS ($h\nu = 833$ eV) and HXPS ($h\nu = 2500$ eV, 4000 eV, and 6000 eV), although all energies were not used for all samples, as specified below. We use pseudocubic notation for the rhombohedral LNO and orthorhombic GTO. The thicknesses are presented in pseudocubic unit cell (u.c.) dimensions, which are 1 u.c. = 3.934 Å for bulk STO with perovskite structure, 1 u.c. = 3.820 Å for bulk LNO with perovskite structure, and 1 u.c. = 3.930 Å for bulk GTO. We note that all films are coherently strained to the LSAT substrate, which changes the unit cell dimensions of the films.

Seven samples consisting of bilayers, trilayers, and MLs were studied, with their configurations given in Table I. The epitaxial STO/LNO superlattice (sample #1) consisted of a bilayer of [3 u.c. STO/4 u.c. LNO] repeated 10 times, as shown in Fig. 1(a). In addition, two bilayers consisting of 2.6 u.c. LNO and 3.7 u.c. LNO on top of a thick layer of STOs (samples #2 and #3, respectively) were grown. All the STO/LNO samples above were deposited by rf magnetron sputtering.⁷

Epitaxial STO/GTO superlattice samples (#4 and #5) consisted of bilayers [8 u.c. STO/2 u.c. GTO] and [5 u.c. STO/2 u.c. GTO] repeated 20 times, respectively, as shown in Fig. 1(b). Sample #5 had in addition a cap layer of 4 u.c. of STO. Two samples consisted of trilayers: #6 = [3 u.c. STO/50 u.c. GTO/3 u.c. STO] and #7 = [4 u.c. STO/8 u.c. GTO/50 u.c. STO] were also grown on top of an LSAT substrate. All STO/GTO samples were deposited by hybrid molecular beam epitaxy.¹¹ Finally, three bulk reference samples of

thickness ≥ 70 nm were grown: #8 = STO, #9 = LNO, and #10 = GTO.

The samples were characterized in several ways^{7,10,11} including transport measurements and transmission electron microscopy (TEM), as reported in other publications.^{7,10} TEM images show that the samples were epitaxial and that their interfaces were sharp, with roughness or interdiffusion between the two constituents of less than one atomic layer. Transport measurements revealed metallic conduction for the superlattices #1 = STO/LNO⁷ and all STO/GTO superlattices.^{10,11}

All SXPS and HXPS data were collected at room temperature in ultra-high vacuum environment (ca. 10^{-9} Torr), without any kind of surface cleaning after atmospheric exposure. The less reactive STO top layers in samples #1, #4, #5, #6, and #7 served to minimize surface reactions and contamination, although STO is known to absorb carbon hydroxide species upon air exposure.²⁰ SXPS experiments were carried out at beamline (BL) 7.0.1 of the Advanced Light Source (LBNL, Berkeley) with a hemispherical electron analyzer (VG Scienta R4000) and a typical energy resolution of 300 meV. The HXPS experiments were performed at three facilities: BLP09 of PETRA III (DESY, Hamburg) with a similar hemispherical analyzer (SPECS Phoibos 225 HV) and resolutions of 400 meV, at BL15XU (Ref. 21) of SPring-8 (Hyogo, Japan), also with a VG Scienta R4000 and resolutions of 240 meV and at BL9.3.1 of the Advanced Light Source (LBNL, Berkeley) with a hemispherical analyzer (Scienta SES 2002) and resolutions better than 600 meV. Energy scales were checked frequently in all cases by measuring the Fermi energy of a Au reference sample. Checking VBO values based on data from one or more of the HXPS facilities showed self-consistency and overall accuracy to within ± 100 meV. Broad-scan survey spectra from some of the HXPS ($h\nu = 5950$ eV) data are shown for STO/LNO superlattice #1 in Fig. 1(a) and for STO/GTO multilayer #4 in Fig. 1(b). These spectra reveal peaks from all of the expected elements, with the only detectable contaminant being a surface layer of carbonaceous material (about 10 Å thick as estimated using the SESSA program²²). We see no evidence in the Sr and Ti core photoelectron spectra of any multiple chemical states, consistent with the previously mentioned stability of STO.

TABLE I. Summary of the experimental values of VBOs as a function of photon energy for several samples of STO/LNO (Nos. 1–3) and STO/GTO (Nos. 4–7). These values are obtained from Eq. (1), where layer A is STO and layer B is LNO or GTO, respectively. The values of the VBOs are positive and the VBM is located higher in binding energy for STO. The VBOs calculated by density functional theory are reported for STO/LNO and STO/GTO.

Sample #		Soft-XPS ($h\nu = 833$ eV) VBO (eV)	Hard-XPS ($h\nu = 2500$ eV) VBO (eV)	Hard-XPS ($h\nu = 4000$ eV) VBO (eV)	Hard-XPS ($h\nu = 6000$ eV) VBO (eV)	Theory VBO (eV)
1	ML [3 u.c. STO/4 u.c. LNO] ₁₀	2.5 \pm 0.3			1.75 \pm 0.05	2.25
2	2.6 u.c. LNO/thick STO	1.5 \pm 0.3				
3	3.7 u.c. LNO/thick STO		1.015 eV	1.025 \pm 0.1		
4	ML [8 u.c. STO/2 u.c. GTO] ₂₀				2.94 \pm 0.05	2.56
5	4 u.c. STO/ML [5 u.c. STO/2 u.c. GTO] ₂₀				3.3 \pm 0.1	
6	3 u.c. STO/50 u.c. GTO/3 u.c. STO				3.5 \pm 0.1	
7	4 u.c. STO/8 u.c. GTO/50 u.c. STO				3.2 \pm 0.1	

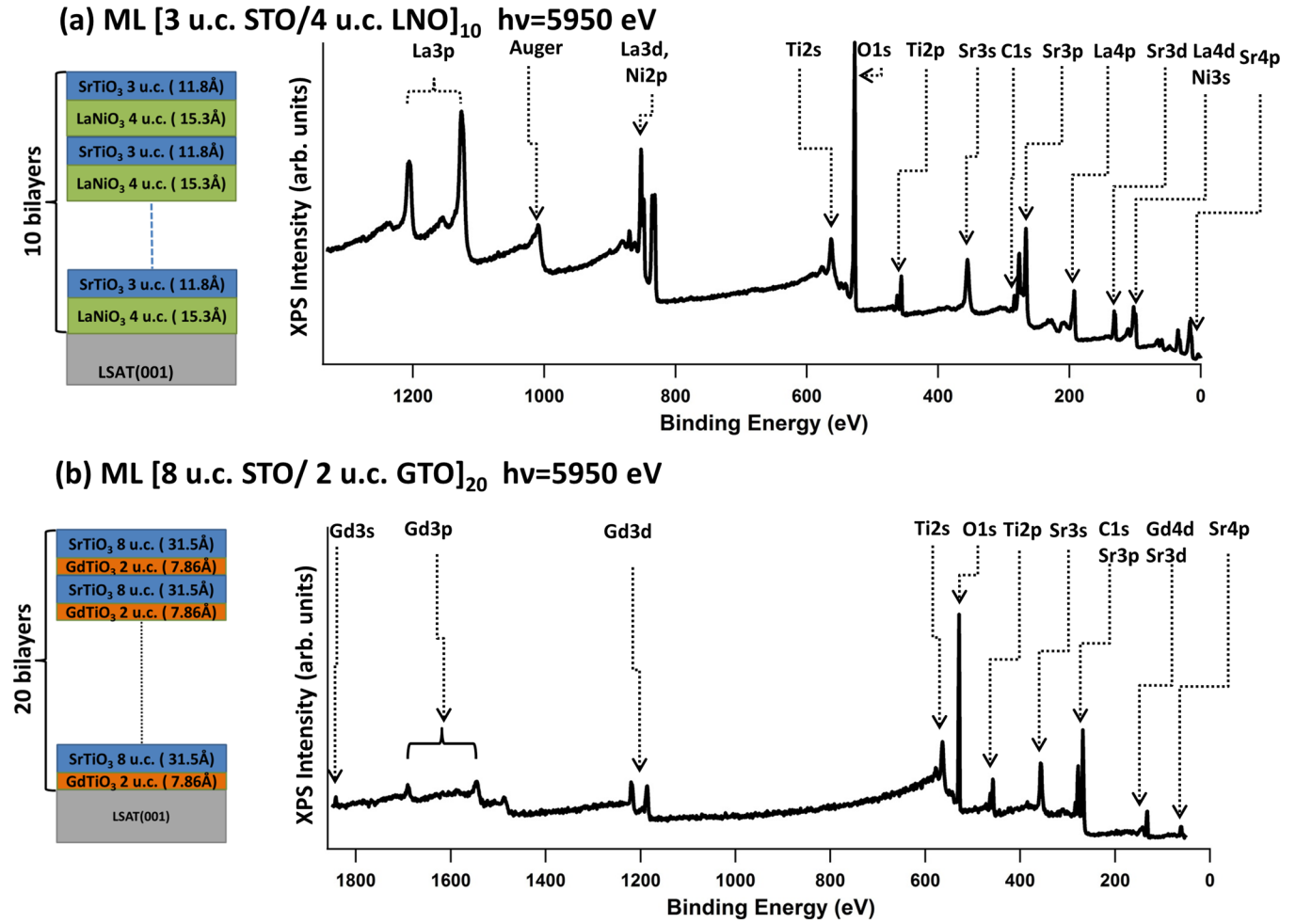


FIG. 1. Schematic of the multilayer samples #1 and #4, together with their associated HXPS survey spectra using excitation at $h\nu = 5950$ eV: (a) from STO/LNO multilayer (#1); (b) from STO/GTO multilayer (#4). Various stronger photoelectron peaks are labeled.

DATA ANALYSIS AND EXPERIMENTAL RESULTS

We applied the XPS VBO method developed initially for semiconductor^{13,14} heterostructures and more recently applied to complex-oxide heterostructures.^{15,16} The basic assumption is that the spectrum of the heterostructures is the superposition of the individual spectra of each layer, with the core levels fixed in energy relative to the local valence-band edge and shifting with it according to the mean local potential near an interface. The VBOs at the STO/LNO or STO/GTO interfaces are thus obtained from the following equation:^{15,16}

$$\Delta E_{VBO}(A/B) = (E_{CL}^{A'} - E_{CL}^{B'}) - [(E_{CL}^A - E_V^A) - (E_{CL}^B - E_V^B)], \quad (1)$$

where ΔE_{VBO} is the VBO of layer A relative to layer B (if positive, the valence bands of A are shifted to higher binding energy compared to those of B, and if negative, they are shifted to lower binding energies), A refers to energies measured in STO and B to energies measured in LNO or GTO, E_{CL}^A is the binding energy of a core level in A, E_V^A is the binding energy of the valence band maximum in A, E_{CL}^B and E_V^B are the same two quantities in B, $(E_{CL}^{A(B)} - E_V^{A(B)})$ are thus the

differences between core-level and valence-band maxima (VBM) for each bulk material A (or B), and $(E_{CL}^{A'} - E_{CL}^{B'})$ is the difference of the same two distinct core-levels chosen for A and B in the heterostructures.

The atomic core level to be used must be unique to a single layer of the superlattice; for instance, we cannot use the Ti2p core level as a reference to determine the STO/GTO band offset, since both STO and GTO contain Ti. In addition, it is important to determine these individual core-level binding energies to an accuracy¹³ of ± 20 meV or better in order to arrive at a $\sim \pm 100$ meV overall error bar for the VBO, whose determination involves several of these binding energies in differences and sums. To achieve this accuracy, the core levels must be as intense and narrow in energy width as possible. Suitable choices that meet these criteria are: Sr 3d and La 4d for STO/LNO and Sr 3d and Gd 3p_{1/2} for STO/GTO, as shown in Fig. 2. The difference between Sr 3d, La 4d, and Gd 3p_{1/2} core levels and their respective VBM binding energies is measured in the bulk STO, bulk LNO, and bulk GTO, respectively, as shown in Figs. 2(a)–2(c) and the separation of the Sr 3d and La 4d, or Sr 3d and Gd 3p_{1/2} is measured in the heterostructures, as shown in Figs. 2(d) and 2(e). After subtracting a Shirley background from the XPS spectra, the core-level peak positions are

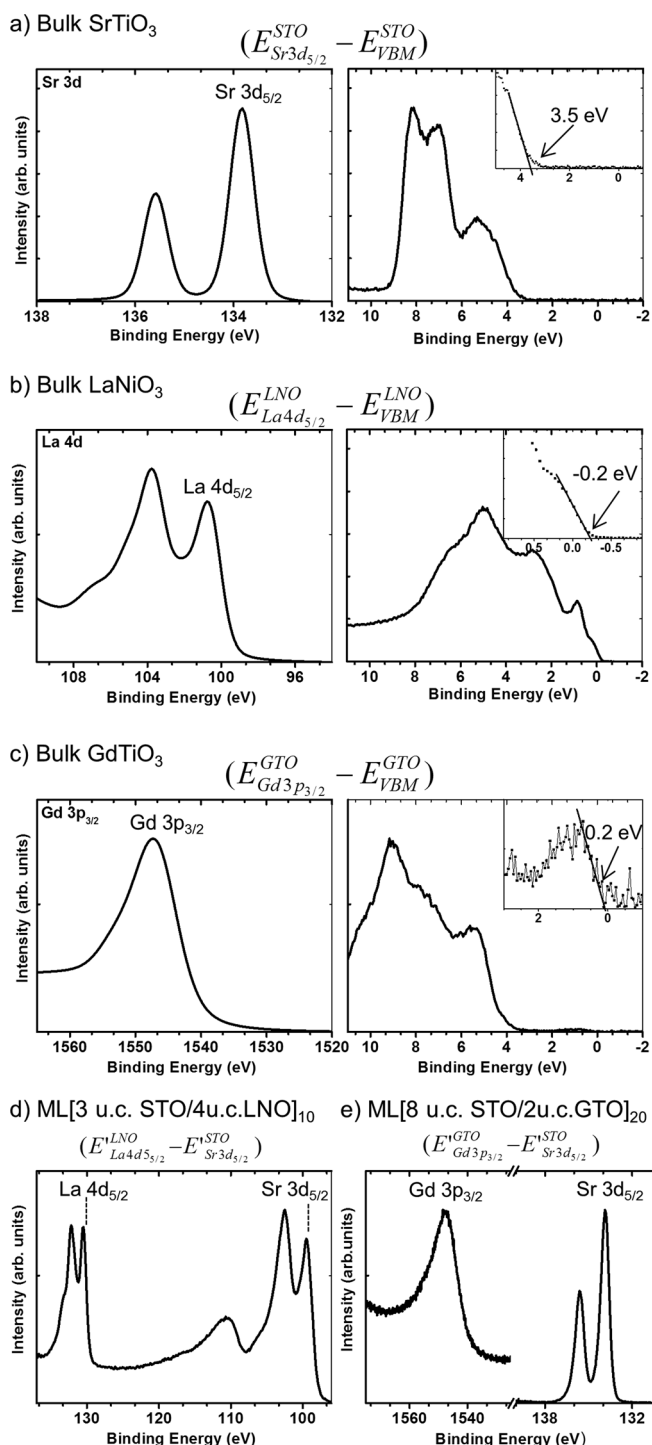


FIG. 2. Examples of determination of key energies for VBO determination via Eq. (1), as related to samples #1 and #4 and with 5950 eV photon energy. (a)–(c) Core- and valence-spectra for bulk reference samples of STO, LNO, and GTO, respectively, with the insets for the valence spectra showing the linear fits used to determine VB maxima. (d) and (e) The differences between reference core levels in two multilayers, STO/LNO, sample #1, and STO/GTO, sample #4.

obtained by fitting these peaks with Voigt functions.²³ This permits finally determining binding energies within about 1/10 of the experimental resolution, or the ± 20 meV mentioned above.

The VBM of STO and LNO bulk samples was determined using a linear regression fit to different sets of data

points along the leading edge of the valence band for STO and LNO bulk samples, as discussed by Chambers *et al.*^{15,16} and is shown in the insets of Figs. 2(b) and 2(c). Chambers *et al.* compared three methods for finding the VBM, and a linear extrapolation method was found to yield more physically reasonable VBM values compared to the other methods. In any case, due to the sensitivity of the VBM to the choice of points on the leading edge used to obtain a regression line, five different sets of points were selected over the linear region of the leading edge to perform regressions. Using this method, we estimate an uncertainty of less than 100 meV for the value of the VBM.

The VBM of GTO is shown in Fig. 2(c). The intense feature below ~ 4 eV is formed by bands of predominantly O 2p character, as verified in the calculations discussed below. The broad feature closer to the Fermi level centered at ~ 1.3 eV is attributed to Ti 3d states.^{24,25} By analogy to the valence band spectra of other strongly correlated titanates,²⁶ this broad peak is identified as the lower Hubbard band (LHB). The VBM for the bulk GTO was defined as the maximum of the LHB.

Before reporting our VBO results, it is important to consider the surface sensitivity of any XPS measurement, especially since the thickness of the topmost STO or LNO layers in our samples ranges from ~ 10 Å to ~ 16 Å. Considering the presence of carbon-containing contamination on the top surface, we estimate that the first STO/LNO or STO/GTO interface is at about 20–26 Å beneath the surface. To be able to measure the band bending at this first interface in the soft XPS regime (with its limited informational depth), we collected data at a photon energy of $h\nu = 833$ eV. The electron inelastic mean free path (IMFP) in STO calculated at a kinetic energy of 833 eV using the TPP-2M formula^{27,28} is about ≈ 16 Å, so we conclude that measuring photoelectrons emanating from the buried interface should be feasible. Other measurements were made at much higher energies, and thus much higher IMFPs, as discussed below.

Measuring the VBOs at such energies with a highly focused soft x-ray synchrotron radiation beam was found to be challenging because of the charge accumulation at the surface when photoelectrons are emitted. As shown in Fig. 3(a), these effects can cause the whole spectrum to shift in time as the charge builds up. One way to correct for this shift is to choose a core level (e.g., C 1s or Sr 3p) as a reference, and to extrapolate the shift to a true zero time, i.e., before charge accumulation (not necessarily the $t = 0$ spectrum) shown in Fig. 3(a). After the core-level peaks are properly aligned and the spectral shift caused by surface charging is corrected, the VBO can be determined. After performing such a correction to the data, we obtain $\Delta E_{\text{VBO}} = 2.5 \text{ eV} \pm 0.3 \text{ eV}$ for the #1 (STO/LNO)₁₀ superlattice and $\Delta E_{\text{VBO}} = 1.5 \text{ eV} \pm 0.3 \text{ eV}$ for the interface STO/LNO in the bilayer #2 = (2.6 u.c.)LNO/STO. However, this method is somewhat cumbersome as well as imprecise, as it assumes a relatively slow and systematic growth of the charging shift in time, which may be true in some cases, but not others. Furthermore, the shifting of spectra on the energy scale can lead to difficulties in resolving different chemical states; and a different degree of charging in different regions of the

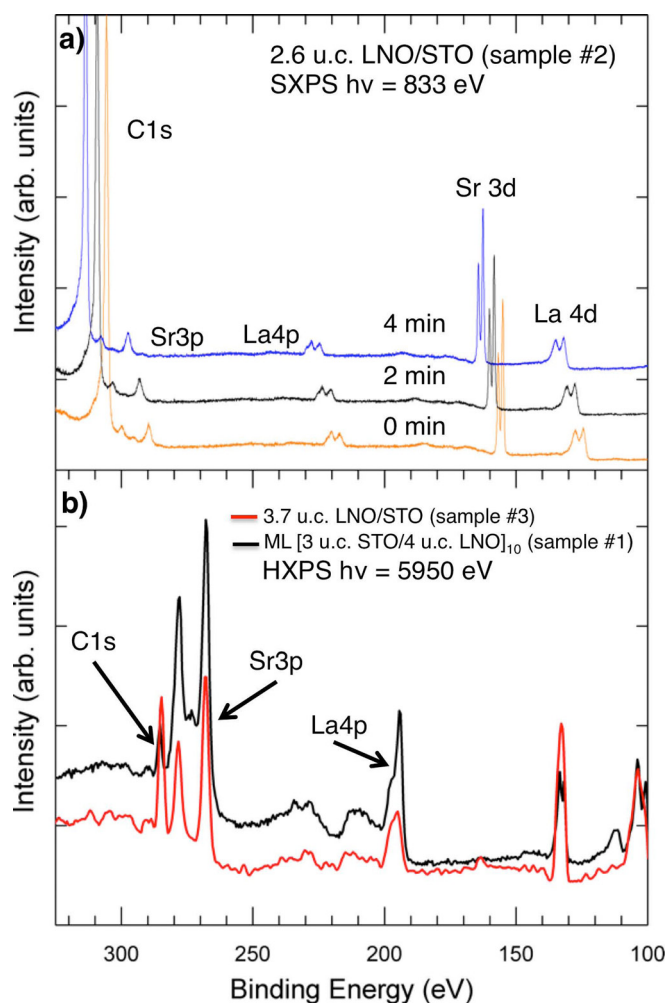


FIG. 3. (a) SXPS spectra at $h\nu = 833$ eV obtained from multilayer STO/LNO sample #2 as a function of time, showing increasing shifts approximately linear in time because of the charge accumulation at the surface. (b) HXPS spectra at $h\nu = 5950$ eV for two samples: bilayer 1.4 nm LNO/STO (#3) and multilayer STO/LNO (sample #1). In (b), the peaks do not shift or broaden with time, indicating reduced or minimal charging problems.

surface may cause a given peak to broaden or to split into more than one peak.

Owing to the detrimental effects mentioned above, it is important to avoid, or at least reduce, charging, which turns out to be possible using HXPS. HXPS provides two advantages: the charging effects have been empirically found to be much reduced, as shown for two other samples in Fig. 3(b), and the probing depth is larger, thus allowing one to probe more than one buried interface in the heterostructure, with less regard for surface contaminants, or surface reaction of the capping layer. The reduction in charging is probably due to the greatly reduced photoelectric cross sections at higher energies, and thus to a lower degree of charging per unit volume, combined with the greater IMFPs, which distribute the region measured over a greater volume. Thus, for some of the samples introduced above, we have measured VBOs at several hard x-ray energies, including 2500 eV, 4000 eV, and 6000 eV.

The values of the VBOs of STO at the interface with LNO and GTO as a function of the XPS photon energies are summarized in Table I and Fig. 4. These results are plotted

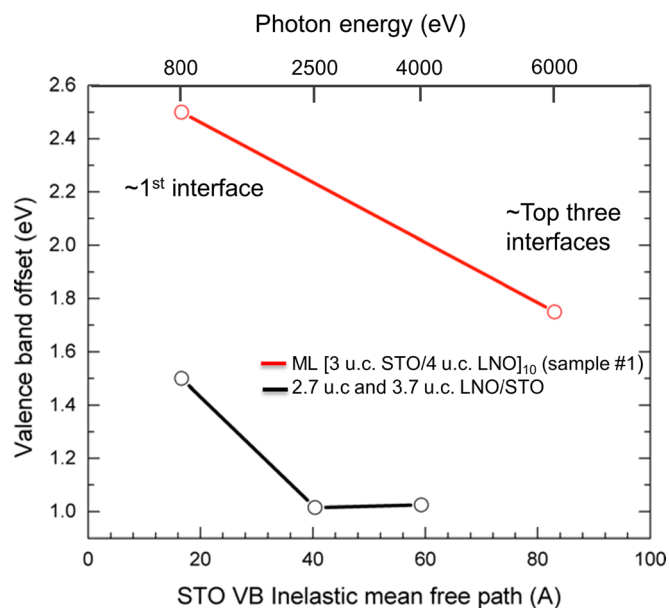


FIG. 4. Valence band offsets as a function of photon energy (top scale) and of IMFP, as calculated by the TPP-2M formula (bottom scale) and measured for the top interfaces of our STO/LNO (#1) and LNO/STO (#2; #3) samples. The number of bilayers and thus interfaces sampled increases with photon energy.

against both photon energy (top scale) and estimated IMFP at that photon energy (bottom scale).^{27,28} Figure 4 shows that the VBOs measured by SXPS and HXPS for the nickelate samples are different for the #1 superlattice. A possible explanation could be that, with SXPS, in addition to a possible experimental error due to the charging problem, there may be an insufficient probing depth to clearly resolve the interface due to the short IMFP ≈ 16 Å. But beyond this, the lower photoelectron energy will emphasize more the region just near the surface of the top layer and the first buried interface, and thus sample the VBO in a different way. A future study in which the VBO of a given system is measured in more detail as a function of photon energy would permit understanding this difference more quantitatively and perhaps also measuring the profile of the band offset as a function of distance from the interface.

As one can see from Fig. 4, the VBOs in the superlattice (#1) are larger by about 1 eV than those of the bilayers (#2 and #3), suggesting enhanced charge buildup at the buried interfaces in the multilayer. A possible explanation of this difference could be that, in the multilayer, STO is on top of LNO, whereas in the bilayers, LNO is on top of STO. A recent paper²⁹ has analyzed position-averaged convergent-beam electron diffraction (PACBED) in scanning transmission electron microscopy to derive the degree of NiO_6 octahedral tilting at the STO/LNO interface, and has shown that epitaxial strain plays a significant role in determining properties such as electrical resistivity and metal-insulator transitions. Thus, we suggest that the different NiO_6 octahedral tilts near the STO/LNO and LNO/STO interfaces could be one of the explanations for the difference in the VBOs between the bilayer and the multilayer, as well as between the soft x-ray and hard x-ray results.

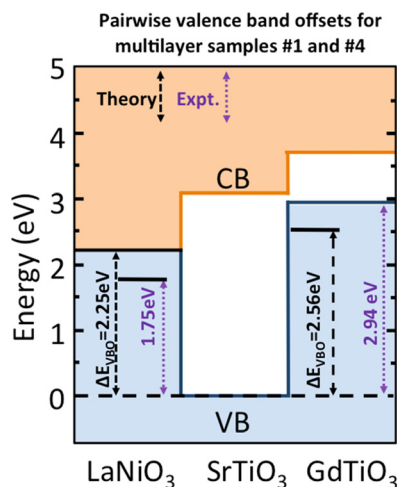


FIG. 5. Direct comparison of theoretical valence band offsets at the STO/LNO and STO/GTO interfaces and experimental HXPS VBOs of the two ML samples #1 and #4. The position of the conduction band minima based on theory and experiment is approximately shown.^{8,9}

Turning now to the STO/GTO samples for which only HXPS ($h\nu \approx 6000$ eV) data were obtained, the VBO values for the two heterostructures are: $\Delta E_{\text{VBO}} = 2.90 \pm 0.05$ eV for multilayer #4 and 3.3 ± 0.1 eV for multilayer #5, which are close to one another. Similar VBO values of 3.5 ± 0.1 eV and 3.2 ± 0.1 eV have been determined for the bilayers #6 and #7, respectively. We note that while the top of the valence band of STO is composed of O 2p states, in GTO it is derived from Ti 3d states, i.e., the top of the lower Hubbard band. For the STO/GTO samples, no SXPS data was collected due to the charging of the bulk GTO sample, which prevented measuring the VBM within even 0.5 eV precision. Thus, an accurate comparison of experiment with theory below is not possible for this case.

FIRST-PRINCIPLES CALCULATIONS OF BAND ALIGNMENTS

Band alignments between STO and LNO or GTO were calculated using density functional theory with a screened hybrid functional^{16,17} and are summarized in Fig. 5. The bulk calculations for STO, LNO, and GTO were performed using 20-atom supercells, whereas the interface calculations were performed for superlattices oriented along the [110] direction; this orientation was chosen in order to avoid effects of charge transfer across the interface in the case of STO/GTO. STO along the [110] direction is composed of alternating planes of $[\text{Sr}^{2+}\text{Ti}^{4+}\text{O}^{2-}]$ and $[(\text{O}^{2-})_2]$, whereas in the case of GTO the alternating planes are $[\text{Gd}^{3+}\text{Ti}^{3+}\text{O}^{2-}]$ and $[(\text{O}^{2-})_2]$. In both cases, the alternating planes have formal charges of 4+ and 4-. Thus, the $(\text{STO})_n(\text{GTO})_n$ superlattices along [110] minimize the effects of polar discontinuity and provide a more accurate representation of the intrinsic band lineup between STO and GTO.

The calculated VBO for the STO/LNO interface is 2.25 eV, which is in reasonable agreement with the experimental values of 2.5 eV in SXPS and 1.75 eV in HXPS for multilayer #1.

For the STO/GTO interface, the first-principles calculations predict 2.56 eV for the VBO, as shown in Fig. 5, again in reasonable agreement with the experiments.

CONCLUSIONS

In summary, we have determined VBOs for several heterostructures of the complex-oxide pairs STO/LNO and STO/GTO, and the values obtained are in good agreement with first-principles calculations based on density functional theory, providing an important link between experiment and theory for such materials. We have also demonstrated that hard x-ray photoemission at ≥ 2 keV is a useful method for determining VBO in complex-oxide superlattices, because charging effects are much reduced, multiple interfaces more characteristic of the “bulk” heterostructure can be probed, and the measurements can be carried out with less regard for surface contaminants or surface reaction on the capping layer than in soft x-ray photoemission at lower energies. The variations of VBOs with photon energy that we see also suggest that future systematic measurements with variable photon energy could be useful for determining the detailed profile of the potential near an interface, providing an additional dimension to VBO studies that may be key in understanding the interface electronic structure, magnetism, and transport properties.

ACKNOWLEDGMENTS

This work was supported by a MURI program of the Army Research Office (Grant No. W911-NF-09-1-0398). The Advanced Light Source, A.B., and W.C.S. are supported by the Director, Office of Science, Office of Basic Energy Sciences, Materials Sciences and Engineering Division, of the U.S. Department of Energy under Contract No. DE-AC02-05CH11231. G.K.P. acknowledges the International Union for Vacuum Science, Technique and Applications and the Swedish Research Council for financial support. P.M. was supported by the U.S. National Science Foundation (Grant No. DMR-1006640). The HXPS measurements at BL15XU of SPring-8 were performed under the approval of NIMS Beamline Station (Proposal No. 2011A4606). S.U., M.K., and K.K. are grateful to HiSOR, Hiroshima University and JAEA/SPring-8 for the development of HXPS at BL15XU of SPring-8. The HAXPES instrument at beamline P09 is jointly operated by the University of Würzburg (R. Claessen), the University of Mainz (C. Felser), and DESY. Funding by the Federal Ministry of Education and Research (BMBF) under contracts 05KS7UM1, 05K10UMA, 05KS7WW3, and 05K10WW1 is gratefully acknowledged. A.J. and C.G.V.d.W. were supported by the US Army Research Office (W911-NF-11-1-0232) and L.B. by the NSF MRSEC Program (DMR-1121053). Computational resources were provided by the XSEDE supported by NSF (OCI-1053575 and DMR07-0072N). A.R. was funded by the Royal Thai Government and C.C. was funded by GAANN program through UC Davis Physics Department.

¹K. Horn, *Appl. Surf. Sci.* **166**, 1 (2000).

²A. Ohtomo and H. Y. Hwang, *Nature* **427**, 423 (2004).

- ³J. Mannhart and D. G. Schlom, *Science* **327**, 1607 (2010).
- ⁴S. D. Ha and S. Ramanathan, *J. Appl. Phys.* **110**, 071101 (2011).
- ⁵W. R. Frensley, in *Chapter 1 of Heterostructures and Quantum Devices*, edited by W. R. Frensley and N. G. Einspruch (VLSI Electronics, 1994).
- ⁶K. van Benthema, C. Elasser, and R. H. French, *J. Appl. Phys.* **90**, 6156 (2001).
- ⁷J. Son, P. Moetaf, J. M. LeBeau, D. Ouellette, L. Balents, S. J. Allen, and S. Stemmer, *Appl. Phys. Lett.* **96**, 062114 (2010).
- ⁸D. A. Crandles, T. Timusk, J. D. Garrett, and J. E. Greedan, *Physica C* **201**, 407 (1992).
- ⁹P. Moetaf, D. G. Ouellette, J. Y. Zhang, T. A. Cain, S. J. Allen, and S. Stemmer, *J. Cryst. Growth* **355**, 166 (2012).
- ¹⁰P. Moetaf, J. Y. Zhang, A. Kozhanov, B. Jalan, R. Seshadri, S. J. Allen, and S. Stemmer, *Appl. Phys. Lett.* **98**, 112110 (2011).
- ¹¹P. Moetaf, T. A. Cain, D. G. Ouellette, J. Y. Zhang, D. O. Klenov, A. Janotti, C. G. Van de Walle, S. Rajan, S. J. Allen, and S. Stemmer, *Appl. Phys. Lett.* **99**, 232116 (2011).
- ¹²J. Auleytner and O. Hornfeldt, *Ark. Fys.* **23**, 165 (1963).
- ¹³E. A. Kraut, R. W. Grant, J. R. Waldrop, and S. P. Kowalczyk, *Phys. Rev. B* **28**, 1965 (1983).
- ¹⁴E. T. Yu, D. H. Chow, and T. C. McGill, *Phys. Rev. B* **38**, 12764 (1988).
- ¹⁵S. A. Chambers, Y. Liang, Z. Yu, R. Droopad, J. Ramdani, and K. Eisenbeiseret, *Appl. Phys. Lett.* **77**, 1662 (2000).
- ¹⁶S. A. Chambers, T. Droubay, T. C. Kaspar, and M. Gutowski, *J. Vac. Sci. Technol. B* **22**, 2205 (2004).
- ¹⁷C. G. Van de Walle and R. M. Martin, *Phys. Rev. B* **34**, 5621 (1986).
- ¹⁸G. Kresse and J. Furthmüller, *Phys. Rev. B* **54**, 11169 (1996).
- ¹⁹J. Heyd, G. E. Scuseria, and M. Ernzerhod, *J. Chem. Phys.* **118**, 8207 (2003); "Erratum," *J. Chem. Phys.* **124**, 219906 (2006).
- ²⁰B. Jalan, J. Cagnon, T. E. Mates, and S. Stemmer, *J. Vac. Sci. Technol. A* **27**, 1365–1368 (2009).
- ²¹S. Ueda, Y. Katsuya, M. Tanaka, H. Yoshikawa, Y. Yamashita, S. Ishimaru, Y. Matsushita, and K. Kobayashi, *AIP Conf. Proc.* **1234**, 403 (2010).
- ²²W. Smekal, W. S. M. Werner, and C. J. Powell, *Surf. Interface Anal.* **37**, 1059 (2005).
- ²³D. A. Shirley, *Phys. Rev. B* **5**, 4709 (1972).
- ²⁴A. Fujimori, I. Hase, M. Nakamura, H. Namatame, Y. Fujishima, Y. Tokura, M. Abbate, F. M. F. de Groot, M. T. Czyzy, J. C. Fuggle, O. Strebel, F. Lopez, M. Domke, and G. Kaindl, *Phys. Rev. B* **46**, 9841 (1992).
- ²⁵M. Sing, M. Karlsson, D. Schrupp, R. Claessen, M. Heinrich, V. Fritsch, H.-A. Krug von Nidda, A. Loidl, and R. Bulla, e-print [arXiv:cond-mat/0205067v1](https://arxiv.org/abs/cond-mat/0205067v1) [cond-mat.str-el].
- ²⁶A. Fujimori, T. Yoshida, K. Okazaki, T. Tsujioka, K. Kobayashi, T. Mizokawa, M. Onada, T. Katsufuji, Y. Taguchi, and Y. Tokura, *J. Electron Spectrosc. Relat. Phenom.* **117–118**, 277 (2001).
- ²⁷S. Tanuma, C. J. Powell, and D. R. Penn, *Surf. Interface Anal.* **21**, 165 (1994).
- ²⁸S. Tanuma, C. J. Powell, and D. R. Penn, *Surf. Interface Anal.* **43**, 689 (2011).
- ²⁹J. Hwang, J. Y. Zhang, J. Son, and S. Stemmer, *Appl. Phys. Lett.* **100**, 191909 (2012).